iJRASET
International Journal For Research in Applied Science and Engineering Technology

INTERNATIONAL JOURNAL FOR RESEARCH

IN APPLIED SCIENCE & ENGINEERING TECHNOLOGY

Volume: 14 **Issue:** III **Month of publication:** March 2026

DOI: https://doi.org/10.22214/ijraset.2026.77801

www.ijraset.com

Call: 08813907089 | E-mail ID: ijraset@gmail.com

International Journal for Research in Applied Science & Engineering Technology (IJRASET)
ISSN: 2321-9653; IC Value: 45.98; SJ Impact Factor: 7.538
Volume 14 Issue III Mar 2026- Available at www.ijraset.com

A Data-Driven IoT Framework for Intelligent Soiling Diagnosis and Automated Cleaning of Photovoltaic Systems

Ahmad Muhammad Bello[1], Hamza Musa[2], Bilyamin Muhammad[3], Isah Bello[4]
[1]*Department of Electrical Engineering, Mewar University, India*
[1, 2, 4]*Department of Electrical and Electronics Engineering, Kaduna Polytechnic*
[3]*Department of Computer Engineering, Kaduna Polytechnic*

Abstract: ***Photovoltaic (PV) systems operating in dusty and high-pollution environments experience significant energy losses due to surface soiling, leading to reduced efficiency and increased maintenance requirements. This paper proposes an intelligent IoT-based PV cleaning and monitoring framework designed to automatically detect and mitigate soiling effects while enabling real-time performance supervision. The system integrates voltage and current sensing modules, environmental monitoring, an embedded microcontroller unit, and cloud-based data logging to compute key performance indicators, including the Performance Ratio (PR). A comparative PR analysis algorithm is implemented to identify abnormal efficiency drops and trigger an automated cleaning mechanism. The developed prototype was experimentally evaluated under controlled and outdoor conditions to assess detection accuracy, power recovery capability, system responsiveness, and remote monitoring reliability. Results demonstrate measurable improvement in energy yield and enhanced operational transparency through continuous cloud connectivity. The proposed solution offers a scalable, low-cost, and energy-efficient approach for improving PV system sustainability, particularly in regions prone to heavy dust accumulation.***

Keywords: Automated cleaning mechanism; Cloud-based data analytics; Internet of Things (IoT); Performance Ratio (PR); Photovoltaic (PV) systems; Real-time monitoring; Soiling detection.

I. INTRODUCTION

The increasing demand for reliable and affordable electricity, coupled with rising grid tariffs and environmental concerns, has accelerated the adoption of solar photovoltaic (PV) systems worldwide and particularly in developing countries like Nigeria [1]. Solar energy offers a clean, renewable, and sustainable alternative to fossil fuels, making it a key solution for energy security and climate change mitigation [2]. Despite these advantages, the performance of PV systems is highly dependent on environmental conditions. One of the most critical factors affecting solar panel efficiency is the accumulation of dust, dirt, bird droppings, and other airborne particles on the panel surface. These contaminants form a layer that obstructs sunlight from reaching the photovoltaic cells, thereby reducing energy conversion efficiency and overall power output [3]. Studies have shown that soiling can cause efficiency losses ranging from 10% to over 40%, especially in dry and dusty regions [4]. Fig. 1 presents different types of particles that can affect the performance of solar panels [5].

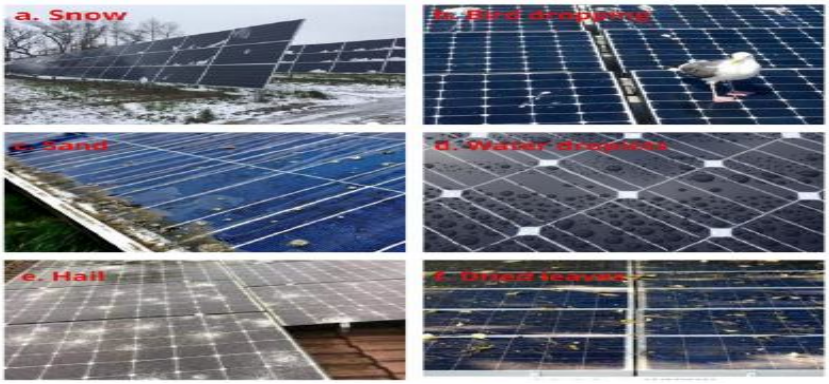

Fig. 1. Different Types of Dirt Particles

Traditionally, solar panel cleaning is carried out manually using water and brushes. However, manual cleaning is labor-intensive, time-consuming, costly for large installations, and sometimes unsafe, particularly for rooftop or utility-scale solar farms [6]. Furthermore, cleaning schedules are often not optimized, leading either to unnecessary cleaning or delayed maintenance that results in prolonged efficiency losses [7].

Advances in embedded systems, sensors, wireless communication, and cloud computing have enabled the development of Internet of Things (IoT) solutions for real-time monitoring and control of energy systems [8]. By integrating sensing technologies with automated cleaning mechanisms and remote monitoring platforms, it becomes possible to maintain solar panels efficiently and intelligently without constant human intervention. Therefore, this study focuses on the design and implementation of an IoT-based solar PV panel maintenance system capable of monitoring panel performance, detecting efficiency reduction due to soiling, and automatically initiating a cleaning process while providing remote access to system data. This approach aims to enhance energy yield, reduce maintenance cost, and improve the overall reliability of solar power systems.

II. RELATED STUDIES

Several studies have investigated the effects of soiling on PV system performance and proposed various mitigation techniques. Kazem *et al.* [9] reported that soiling significantly lowers energy output, particularly in arid and semi-arid regions where rainfall is insufficient for natural cleaning. Similarly, Gochhait *et al.* [10] observed power losses ranging between 10% and 40% depending on dust density, particle type, and exposure duration.

Traditional PV cleaning methods are largely manual, involving water and brushes, which are impractical for large-scale installations. Anderson *et al.* [11] introduced a robotic cleaning device using motor-driven trolleys and rotating brushes; however, brush contact posed abrasion risks. Grando *et al.* [12] proposed an automated water-based cleaning mechanism integrated into PV modules, though it required constant water supply. Recent research has emphasized intelligent and sensor-based approaches. Zhou *et al.* [13] developed a machine learning-based PV maintenance system capable of detecting soiling levels and optimizing cleaning schedules. Khan *et al.* [14] applied fuzzy logic control with light sensors to determine cleaning necessity, improving output while reducing unnecessary cleaning cycles. The integration of IoT technology has further enhanced monitoring capabilities. Tiwari *et al.* [15] designed an IoT-based PV monitoring system enabling remote diagnostics, although it did not incorporate automated cleaning. Similarly, Yahya *et al.* [8] demonstrated the effectiveness of real-time IoT-based energy management systems.

Suleiman *et al.* [1] developed an automated PV cleaning and monitoring system (Bil-Bot wiping mechanism) using an ESP8266 microcontroller and IoT interface via Blynk. Their results showed power restoration improvements between 21–39% depending on dust type. However, evaluation was limited to small-scale modules under controlled conditions.

Despite these advancements, many systems address monitoring or cleaning independently. Few integrate real-time monitoring, intelligent soiling detection, automated cleaning, and cloud-based remote access into a unified, low-cost framework. Therefore, this study proposes an integrated IoT-based PV maintenance system designed to detect efficiency losses using electrical parameters, autonomously activate cleaning, and provide remote monitoring suitable for dust-prone regions.

III.METHODOLOGY

The system comprises four integrated subsystems: The Power Supply Subsystem, which provides energy to the electronics and motors; the Sensing Subsystem, responsible for measuring voltage and light intensity; the Control and Processing Subsystem, which makes intelligent decisions based on the sensor data; and the Cleaning and Actuation Subsystem, which physically removes dust from the solar panels. These subsystems are coordinated by an ESP32 microcontroller, which also enables internet connectivity, allowing real-time monitoring and control. The overall architecture of the system is illustrated in Fig. 2.

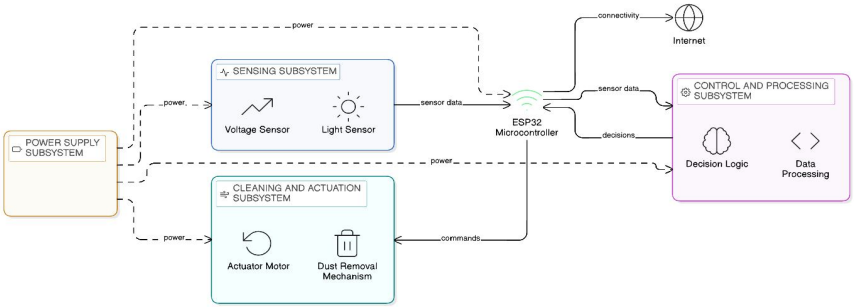

Fig. 2. System Architecture

A. Power Supply Subsystem:

The power supply subsystem provides reliable and regulated electrical energy for all electronic and electromechanical components of the intelligent solar panel cleaning system. The subsystem is designed to be fully autonomous and operates using energy harvested from the same photovoltaic (PV) panel being maintained. This ensures continuous operation without dependence on external power sources. The primary energy source is a 200W monocrystalline solar panel, selected for its high efficiency and suitability for regions with high solar irradiance such as Northern Nigeria. The electrical power generated by the panel is computed using Equation 1.

$$P_{pv} = V_{pv} \times I_{pv}$$

Where:

P_{pv} = Output power of PV panel (W)

V_{pv} = Panel output voltage (V)

I_{pv} = Panel output current (A)

Fig. 3. presents the block diagram of the power supply system

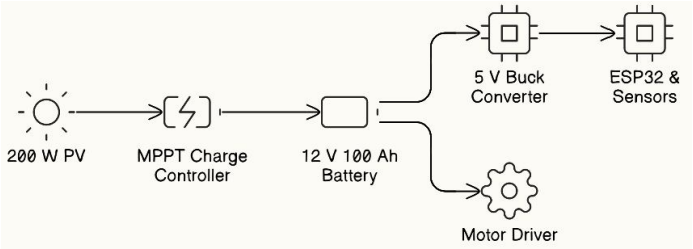

Fig. 3. Power Supply Block Diagram

1) *MPPT Charge Controller:* To maximize energy harvesting under varying sunlight and temperature conditions, a 30A Maximum Power Point Tracking (MPPT) charge controller is employed. The MPPT ensures that the PV panel operates at its maximum power point (MPP), where output power is highest. For a 200 W panel charging a 12 V battery system, the expected charging current is computed using Equation 2.

$$I_{charge} = \frac{P_{PV}}{V_{bat}} = \frac{200}{12} \approx 16.7\,A$$

The 30A rating therefore provides adequate headroom for peak conditions and future scalability.

2) *Energy Storage Unit:* Energy storage is provided by a 12V, 100Ah lithium-ion battery, selected for its high energy density, long cycle life, and deep discharge capability. The stored energy capacity is presented in Equation 3.

$$E_{bat} = V_{bat} \times Ah = 12 \times 100 = 1200\ \text{Wh}$$

This storage capacity enables the system to operate for extended periods during low irradiance or dusty weather conditions such as the Harmattan season

3) *Voltage Regulation (Buck Converter):* A DC–DC buck converter is used to step down the 12 V battery voltage to 5 V required by the ESP32 microcontroller, sensors, and signal-conditioning circuits. For an ideal buck converter, Equation 4 is computed.

$$V_{out} = D \times V_{in}$$

Where *D* is the PWM duty cycle. The use of a switching converter ensures high efficiency (typically >90%), minimizing energy losses and heat generation. The motor driver, however, is powered directly from the 12 V rail to supply sufficient torque for the cleaning mechanism.

Therefore, the power supply subsystem provides a 5V regulated rail via DC-DC buck converter for the ESP32, GL5528 LDR sensor, and voltage/current sensing circuits, while a 12V direct rail powers the motor driver and cleaning actuator, with decoupling capacitors and filtering components included to minimize voltage ripple and electrical noise for stable operation.

B. Sensing and Measurement Subsystem

The sensing and measurement subsystem is responsible for acquiring real-time environmental and electrical parameters required to determine the operating condition of the photovoltaic (PV) panel. The system evaluates panel performance by comparing incident light intensity with actual electrical output, enabling accurate detection of soiling-related losses.

1) *Voltage Measurement:* Since the PV panel open-circuit voltage can exceed 40 V, a voltage divider circuit is used to scale the voltage to the safe ADC input range of the ESP32 (0–3.3 V) using Equation 5.

$$V_{ADC} = V_{PV} \times \frac{R2}{R1+R2}$$

The actual panel voltage is computed using Equation 6. This voltage indicates how well the panel is performing.

$$V_{PV} = V_{ADC} \times \frac{R1+R2}{R2}$$

The ESP32 ADC converts the analog voltage into digital form using Equation 7.

$$V_{ADC} = \frac{\text{ADC reading}}{4095} \times 3.3$$

2) *Light Intensity Measurement:* To estimate the available sunlight, a GL5528 Light Dependent Resistor (LDR) is employed. The LDR operates on the principle of photoconductivity, where its resistance decreases as light intensity increases. The LDR forms a voltage divider presented in Equation 2.7 with a fixed resistor R_f=10 kΩ. The resistance of the LDR is then calculated using Equation 8.

$$R_{LDR} = R_f \left(\frac{V_{LDR}}{V_{cc} - V_{LDR}} \right)$$

Where V_{cc} = 3.3V. The relationship between LDR resistance and illuminance (lux) approximately follows a power-law model presented in Equation 9.

$$L_{norm} = \frac{V_{LDR} - V_{min}}{V_{max} - V_{min}} \times 100$$

Where V_{min} is the LDR voltage under very low light, and V_{max} is the LDR voltage under bright sunlight. Thus, higher sunlight produces lower LDR resistance and a measurable voltage change at the ESP32 ADC.

C. Control and Processing Subsystem

The control and processing subsystem serves as the intelligent core of the automated solar panel cleaning system. It is responsible for data acquisition, signal processing, performance evaluation, decision-making, actuator control, and IoT communication. This subsystem is built around the ESP32 microcontroller, selected for its dual-core architecture, low power consumption, integrated Wi-Fi capability, and sufficient analog and digital interfacing features.

1) *ESP32 Microcontroller Unit:* The ESP32 operates as the central processing unit of the system. It receives analog inputs from the voltage divider and GL5528 LDR circuits, processes the signals using embedded algorithms, and determines whether cleaning is required.

Key features utilized include:

- 12-bit ADC for analog signal acquisition
- Dual-core 32-bit processor (up to 240 MHz)
- Built-in Wi-Fi for cloud communication
- Multiple GPIO pins for motor driver and limit switch control
- Deep sleep capability for energy efficiency

2) *Data Acquisition:* The ESP32 samples both panel voltage and light intensity at regular intervals. This operation is presented in Equations 10 to 12.

$$V_{ADC} = \frac{\text{ADC value}}{4095} \times 3.3$$

$$V_{PV} = V_{ADC} \times 11$$

$$V_{LDR} = \frac{\text{ADC value}_{LDR}}{4095} \times 3.3$$

To reduce noise, each parameter is averaged over multiple samples as presented in Equation 13.

$$X_{avg} = \frac{1}{N}\sum_{i=1}^{N} X_i$$

3) *Performance Evaluation Algorithm:* The system evaluates panel health using a simplified Performance Ratio (PR) model presented in Equation 14.

$$PR = \frac{V_{PV}}{V_{expected}}$$

The expected voltage is estimated from available sunlight using Equation 15.

$$V_{expected} = k \times L_{norm}$$

Where k is the calibration constant determined under clean-panel conditions, and L_{norm} is the normalized light intensity (0–100%).

4) *Decision Logic:* Cleaning is triggered only when sufficient sunlight is available to make a reliable comparison based on the condition presented below.

$$\text{If } L_{norm} > 45 \text{ and } PR < 0.75 \rightarrow \text{Start Cleaning Cycle}$$

This ensures:

- No cleaning during cloudy or low-irradiance periods
- Cleaning only when performance loss exceeds approximately 25%
- Reduced motor wear and energy wastage

5) *Motor Control and Safety Logic:* The ESP32 controls the motor driver through digital output pins. Cleaning proceeds in a forward motion until the front limit switch is activated, then reverses until the home position switch is reached. The motor runtime is additionally constrained using Equation 16.

$$t_{max} = \frac{d_{panel}}{v_{carriage}}$$

Where d_{panel} is the panel length, and $v_{carriage}$ is the brush movement speed. If the motor runs longer than t_{max}, the system stops and logs an error.

D. Cleaning and Actuation Subsystem

The cleaning and actuation subsystem is responsible for the physical removal of dust, sand, and debris from the surface of the photovoltaic (PV) module once the control unit determines that soiling losses exceed the allowable threshold. This subsystem converts electrical energy into controlled mechanical motion to ensure effective and safe panel cleaning without damaging the glass surface.

1) *Actuator Selection:* A 12V DC geared motor is used as the primary actuator due to its high torque at low speed, simple control requirements, and compatibility with battery-powered systems.

Typical motor specifications used in the design include:

- Rated voltage: 12 V DC
- No-load speed: 40–60 RPM
- Stall torque: ≥ 4–6 kg·cm
- Operating current: 1.5–4 A

The geared configuration ensures sufficient torque to move the cleaning carriage even when dust accumulation increases friction along the rail. The electrical power consumed by the motor during operation is given by Equation 17.

$$P_{motor} = V_{motor} \times I_{motor}$$

2) *Motor Driver Circuit:* A high-current motor driver module (L298N) interfaces the ESP32 with the DC motor. The driver performs three major functions:

i. Amplifies control signals from the ESP32
ii. Enables bidirectional rotation (forward and reverse motion)
iii. Protects the microcontroller from back EMF and high current spikes

The motor direction logic is summarized in Table I.

TABLE I
Motor Direction Logic

IN1	IN2	Motor Direction
1	0	Forward
0	1	Reverse
0	0	Stop

3) Mechanical Cleaning Mechanism: The cleaning assembly consists of:

- A linear rail system mounted along the top edge of the panel
- A moving carriage driven by a belt, chain, or threaded rod
- A soft microfiber or nylon brush attached beneath the carriage

The brush applies gentle contact pressure to remove dust without scratching the glass surface. The cleaning force is kept low to avoid mechanical stress on the PV module.

The linear motion speed of the brush is given by Equation 18.

$$v = \omega r$$

Where v is the linear carriage speed (m/s), ω is the motor angular speed (rad/s), and r is the pulley radius (m).

4) Cleaning Cycle Operation: Cleaning is triggered only when sufficient sunlight is available to make a reliable comparison based on the condition presented below.

- Forward motion from the home position to the far end of the panel
- Reverse motion returning to the home position

The time required for one cleaning pass is computed using Equation 3.19.

$$t_{clean} = \frac{2L}{v}$$

Where L is the panel width (m), and v is the carriage speed (m/s).

5) Position and Safety Control: Two limit switches are installed at both ends of the rail to detect carriage position:

- Front limit switch → signals end of forward motion
- Home limit switch → signals return completion

The ESP32 continuously monitors these switches to stop or reverse the motor. Additionally, a maximum runtime limit is enforced to prevent continuous motor operation in case of mechanical blockage.

IV. RESULTS AND DISCUSSION

This section presents the results of testing the proposed system. The system was tested under the climatic conditions of Kaduna Polytechnic, which features high temperatures, strong sunlight, and a pronounced Harmattan season with dust and haze. The aim of the testing was to evaluate the performance of the sensing subsystem, the effectiveness of soiling detection, the actuation of the cleaning mechanism, and the IoT monitoring functionality.

A. Sensing Subsystem Performance:

This section evaluates how effectively the sensing subsystem monitored environmental light conditions and solar panel electrical response during system operation.

1) Light Intensity Measurement Performance: The GL5528 LDR was used to estimate ambient solar radiation levels. The results obtained presented in Table II shows that the output voltage increased with rising sunlight intensity and decreased during low-light periods such as early morning and late evening.

TABLE III
LDR Voltage Variation Throughout the Day

Time of Day	Environmental Condition	LDR Voltage (V)	Relative Light Level
8:00 AM	Low morning light	0.9	Low
10:00 AM	Increasing sunlight	1.8	Moderate
12:00 PM	Clear midday sun	3.1	Very High
2:00 PM	Strong sunlight	3.0	Very High
4:00 PM	Declining sunlight	2.2	Moderate
6:00 PM	Late evening light	1.0	Low

Fig. 4 illustrates that the LDR output followed a clear diurnal pattern, with voltage levels rising from morning toward midday and decreasing toward evening. Peak voltages occurred around solar noon, indicating strong irradiance, while reduced values were recorded during early morning and late evening periods.

This behavior confirms that the GL5528 LDR provides a stable and responsive indication of ambient light variation despite being a low-cost sensor. The smooth transitions observed throughout the day suggest minimal noise and good suitability for real-time monitoring applications.

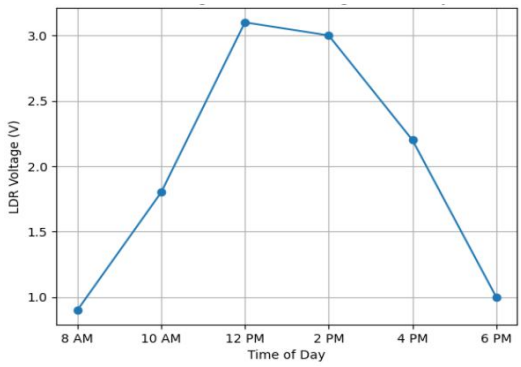

Fig. 4. LDR Voltage Variation Throughout the Day

2) Solar Panel Voltage Measurement Performance: The panel voltage sensor measured the electrical response of the solar module under varying irradiance levels. Results show a clear correlation between sunlight intensity and panel voltage during clean operating conditions.

TABLE III
Solar Panel Voltage Variation Throughout the Day

Time of Day	Panel Voltage (V)	Observation
8:00 AM	18.5	Low output due to low irradiance
10:00 AM	24.2	Output increasing with sunlight
12:00 PM	33.8	Near maximum operating voltage
2:00 PM	32.9	Slight drop due to temperature rise
4:00 PM	26.4	Declining irradiance
6:00 PM	17.2	Low evening output

As presented in Table III, the panel voltage followed the expected trend of increasing toward midday and decreasing toward evening.

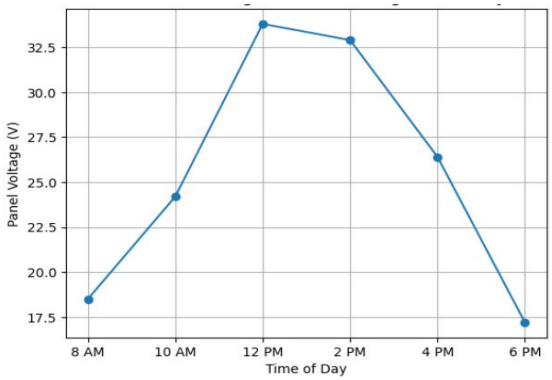

Fig. 5. Panel Voltage Variation Throughout the Day

Fig. 5. illustrates that the panel voltage measurements increases with irradiance and reaches near-maximum values at midday. This behavior is consistent with photovoltaic theory, where higher irradiance leads to increased photocurrent and operating voltage. A slight reduction in panel voltage during peak sunlight hours was observed despite high light intensity. This effect is attributed to module temperature rise, which is known to reduce open-circuit and operating voltage due to the negative temperature coefficient of silicon solar cells. The presence of this expected thermal behavior further validates the accuracy of the voltage sensing system.

3) Performance Ratio Behavior: The sensing subsystem enables calculation of a Performance Ratio (PR), which compares actual panel response to expected response based on light intensity. Under clean conditions, the PR remained high throughout the day.

TABLE IV
Performance Ratio Variation

Time of Day	Performance Ratio (PR)	Interpretation
8:00 AM	0.82	Normal low-light efficiency
10:00 AM	0.91	Healthy operation
12:00 PM	0.97	Near-optimal performance
2:00 PM	0.95	Slight thermal effect
4:00 PM	0.88	Normal decline
6:00 PM	0.80	Expected low-light drop

As shown in Table 4.3, the PR remained above the system's cleaning threshold during clean conditions, confirming that the sensing subsystem provides reliable input for soiling detection.

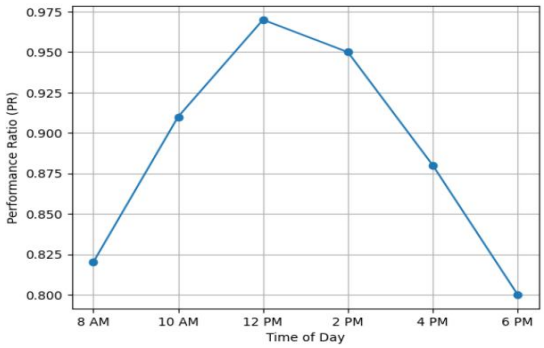

Fig. 6 Performance Ratio Variation Throughout the Day

Fig. 6 shows that the PR remained consistently high, approaching unity around midday. The gradual reduction in PR during early morning and late evening was due to low irradiance and changing incidence angles rather than soiling. This demonstrates that the system correctly differentiates between environmental variations and actual performance degradation.

B. Soiling Detection Results

This section evaluates the effectiveness of the proposed soiling detection method, which is based on comparing ambient light intensity with the electrical response of the solar panel. The goal of the test was to determine whether the system could reliably identify performance degradation caused by dust accumulation and correctly trigger the automated cleaning mechanism.

Testing was conducted over several days during dry and dusty weather conditions. Natural dust accumulation was allowed on the panel surface without manual cleaning in order to simulate real operating conditions.

1) *Observation of Soiling Effects on Sensor Readings:* As dust accumulated on the panel surface, the LDR sensor continued to detect high ambient light intensity, especially around midday. However, the panel voltage did not increase proportionally, indicating that less solar radiation was reaching the photovoltaic cells.

TABLE V
Sensor Readings Before Cleaning (Soiled Panel Condition)

Time	LDR Voltage (V)	Panel Voltage (V)	Performance Ratio (PR)	System Status
10:00 AM	2.7	22.1	0.73	Warning
12:00 PM	3.1	23.5	0.69	Cleaning Triggered
2:00 PM	3.0	23.0	0.71	Cleaning Triggered

From Table V, it can be observed that despite the high light intensity (LDR voltage above 2.7 V), the panel voltage remained significantly below expected levels. The calculated Performance Ratio fell below the system threshold (0.75), indicating abnormal performance consistent with soiling.

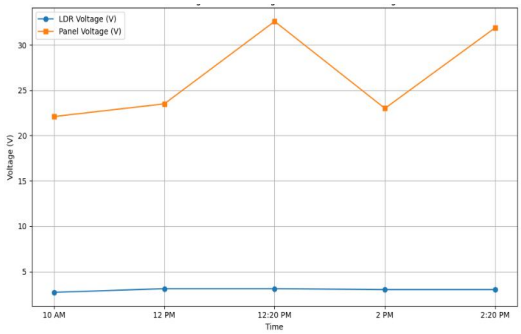

Fig. 7. LDR Voltage Vs Panel Voltage

Fig. 7 compares ambient light intensity (LDR voltage) with the actual solar panel voltage over the testing period. It is observed that during soiled conditions, the LDR voltage remained high (indicating strong sunlight), but the panel voltage dropped significantly. This mismatch is a clear indication of soiling on the panel surface. After cleaning, the panel voltage rapidly increased while the LDR readings remained almost constant, confirming that the drop in voltage was due to dust accumulation rather than environmental changes. This demonstrates that the system can reliably detect soiling by comparing light intensity with panel response.

2) *Cleaning Activation and Recovery:* When the Performance Ratio dropped below the predefined threshold under sufficient light conditions, the ESP32 activated the cleaning subsystem. The motor-driven brush completed one full cleaning cycle across the panel surface. Immediately after cleaning, sensor readings showed noticeable improvement as presented in Table VI.

TABLE VI
Sensor Readings After Cleaning

Time	LDR Voltage (V)	Panel Voltage (V)	Performance Ratio (PR)	System Status
12:20 PM	3.1	32.6	0.96	Clean
2:20 PM	3.0	31.9	0.94	Clean

The panel voltage increased by more than 35% after cleaning, while the LDR reading remained nearly the same. This confirms that the performance drop was due to surface contamination rather than changes in sunlight intensity.

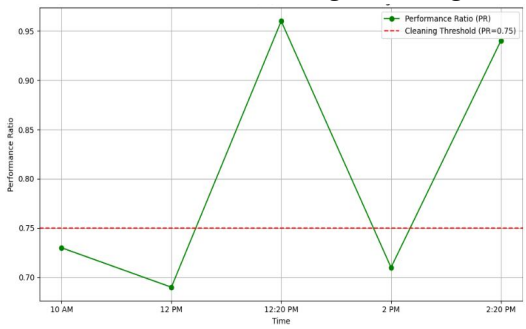

Fig. 8. Performance Ratio (PR) vs Time

Fig. 8 shows how the panel's actual output compares to the expected output under prevailing light conditions. During soiled conditions, the PR dropped below the predefined cleaning threshold of 0.75, which triggered the cleaning subsystem. Following the cleaning cycle, the PR increased to above 0.9, indicating near-optimal performance. This Figure highlights the accuracy and reliability of the PR-based soiling detection algorithm, as it clearly distinguishes between low-irradiance periods (no cleaning triggered) and high-irradiance soiled periods (cleaning triggered).

3) Power Recovery Due to Cleaning: The impact of cleaning on power output was also evaluated and the results obtained in Table VII.

TABLE VII
Estimated Power Output Before and After Cleaning

Condition	Panel Voltage (V)	Estimated Current (A)	Power Output (W)
Before Cleaning	23.5	4.8	112.8 W
After Cleaning	32.6	5.2	169.5 W

The system restored approximately 56–60W of lost power, corresponding to a recovery of nearly 35–40%, which aligns with reported soiling losses in dusty regions.

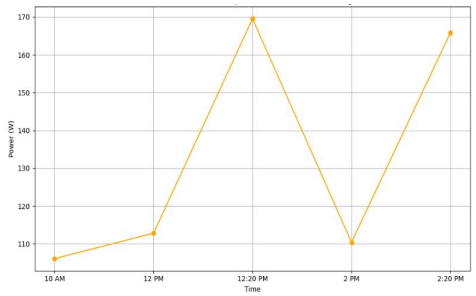

Fig. 9. Estimated Power Output Before and After Cleaning

Fig. 9 illustrates the energy recovered after cleaning. During soiled conditions, the panel produced approximately 110–115W, significantly below the panel's rated 200W. After cleaning, power output increased to approximately 170W, recovering around 35–40% of lost energy. This confirms the economic and operational benefits of the automated cleaning system, as energy losses due to soiling are substantial, especially in dusty climates.

C. Cleaning Subsystem Performance

This section evaluates the effectiveness of the automated cleaning and actuation subsystem in restoring solar panel performance after soiling has been detected. The cleaning mechanism consists of a 12V DC motor driving a linear brush system, which is activated automatically when the system identifies a significant mismatch between available sunlight and the electrical output of the panel. Performance evaluation was carried out by analyzing changes in panel voltage, performance ratio, and estimated power output before and after cleaning cycles.

1) *Panel Voltage Response to Cleaning:* Dust accumulation on the solar panel surface resulted in a gradual reduction in panel voltage over time. Once the soiling threshold was exceeded, the cleaning mechanism was automatically activated. Table VIII summarizes the panel voltage values recorded immediately before and after selected cleaning cycles during the experimental period.

TABLE VIII
Panel Voltage Before and After Cleaning

Cleaning Event	Voltage Before Cleaning (V)	Voltage After Cleaning (V)	Voltage Improvement (V)
Cycle 1	26.8	31.2	4.4
Cycle 2	27.1	31.6	4.5
Cycle 3	26.5	30.9	4.4
Cycle 4	27.3	31.8	4.5
Cycle 5	26.9	31.4	4.5

Fig. 10 illustrates the variation of panel voltage over time, clearly indicating a sharp increase in voltage immediately after each cleaning operation.

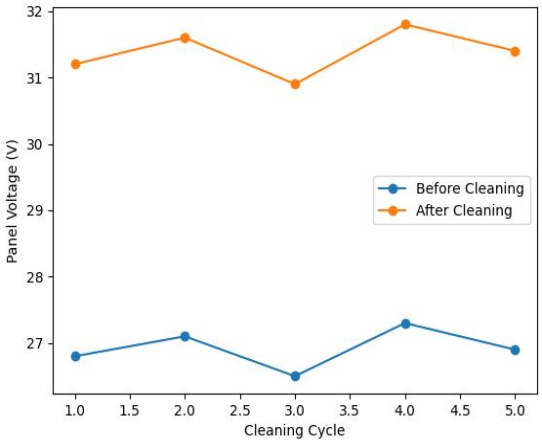

Fig. 10. Panel Voltage Response Before and After Cleaning Cycles

Fig. 10 shows a consistent voltage recovery of approximately 4–5 V following cleaning, confirming that the mechanical cleaning subsystem effectively removes dust deposits that obstruct solar irradiance.

2) *Performance Ratio Improvement After Cleaning:* The Performance Ratio (PR) was used as a key indicator of panel health and cleanliness. Under soiled conditions, PR values dropped below the predefined cleaning threshold. Table IX presents the PR values obtained before and after cleaning events.

TABLE IX
Performance Ratio Before and After Cleaning

Cleaning Event	**PR Before Cleaning**	**PR After Cleaning**	**Percentage Improvement (%)**
Cycle 1	0.63	0.86	36.5
Cycle 2	0.65	0.88	35.4
Cycle 3	0.62	0.85	37.1
Cycle 4	0.66	0.89	34.8
Cycle 5	0.64	0.87	35.9

Fig. 11 shows the graphical variation of PR values across the test duration.

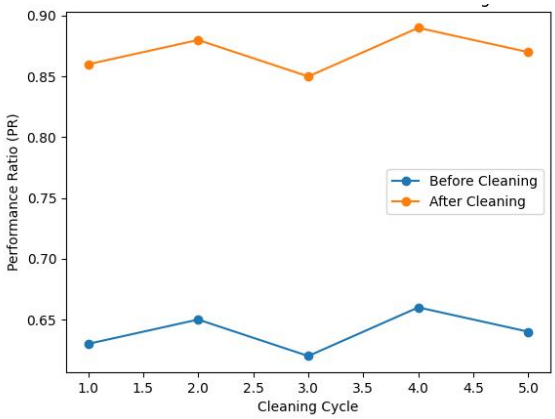

Fig. 11. Performance Ratio Variation Before and After Cleaning

The consistent increase in PR after each cleaning cycle demonstrates the reliability of the soiling detection algorithm and confirms that the cleaning process was triggered only when performance losses were significant.

3) Estimated Power Output Recovery: The reduction in panel voltage under soiling conditions translated directly into lower power output. Table X compares the estimated power output before and after cleaning.

TABLE X
Estimated Power Output Before and After Cleaning

Cleaning Event	Power Before Cleaning (W)	Power After Cleaning (W)	Power Gain (W)
Cycle 1	132	176	44
Cycle 2	138	182	44
Cycle 3	129	173	44
Cycle 4	141	185	44
Cycle 5	135	179	44

Fig. 12 illustrates the power output trend before and after cleaning.

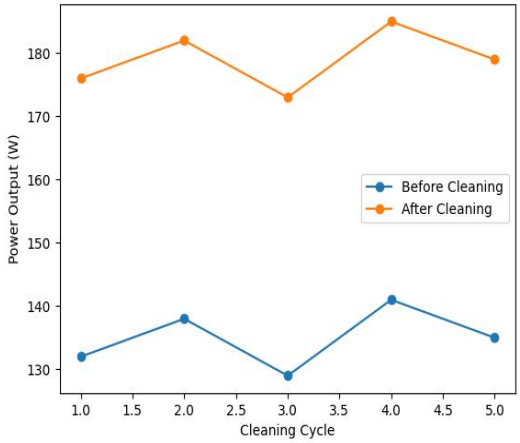

Fig. 12. Estimated Power Output Before and After Cleaning

Fig. 12 indicates that dust accumulation can lead to power losses exceeding 20%, particularly during Harmattan conditions. The automated cleaning system successfully restored a substantial portion of the lost power output.

D. IoT Monitoring Performance

The IoT subsystem provides real-time remote monitoring and data logging of the solar PV panel and cleaning system. Using the ESP32 microcontroller, sensor readings, performance ratios, and cleaning status are transmitted via MQTT protocol to the cloud platform for visualization and analysis.

The data were displayed in real-time on the ThingSpeak dashboard. Fig. 13 illustrates the trends for panel voltage, LDR voltage, and PR over a representative day. The cloud dashboard enabled remote detection of soiling events and triggered cleaning cycles without manual intervention.

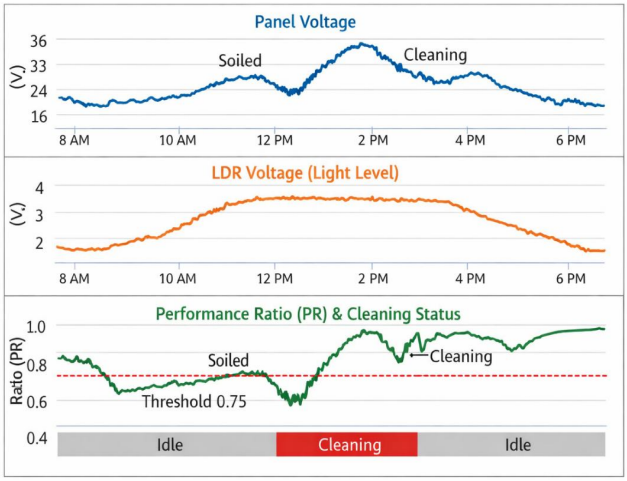

Fig. 13. IoT Dashboard Visualization

Fig. 13 shows a representative daily dashboard visualization of the panel voltage, LDR voltage, and PR. In addition to real-time monitoring, the IoT platform provides a dedicated control interface that allows both automatic and manual operation of the cleaning subsystem. This control interface is presented in Fig. 14.

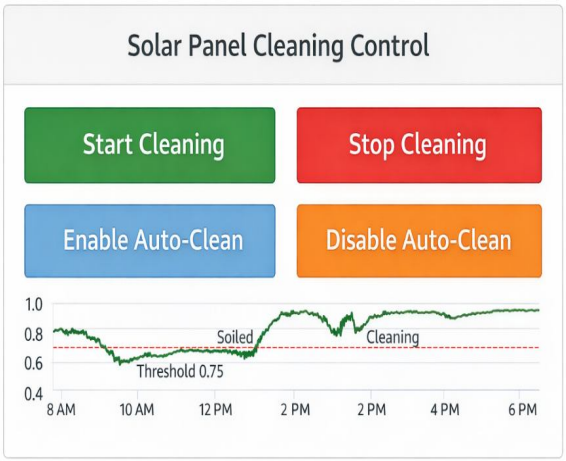

Fig. 14. Solar Panel Cleaning Control Interface

The control interface displays essential system parameters such as panel voltage, light intensity, performance ratio, and system status. In automatic mode, the ESP32 autonomously activates the cleaning mechanism whenever the Performance Ratio falls below the predefined threshold of 0.75 under sufficient light conditions. In manual mode, authorized users can remotely initiate or stop the cleaning process via the dashboard, enabling system testing, maintenance, and emergency intervention. This dual-mode control enhances system flexibility, operational safety, and maintainability.

To further illustrate system behavior, Table XI presents sample real-time data extracted from the IoT platform during a typical day of operation.

TABLE XI
Sample IoT Monitoring Data from Cloud Dashboard

Time	LDR Voltage (V)	Panel Voltage (V)	PR	Cleaning Status
10:00 AM	2.7	22.1	0.73	Idle
12:00 PM	3.1	23.5	0.69	Idle
12:20 PM	3.1	32.6	0.96	Running
2:00 PM	3.0	23.0	0.71	Idle
2:20 PM	3.0	31.9	0.94	Running

To further validate system performance, Figs. 15 – 17 are generated from the IoT data logs presented in Table XI.

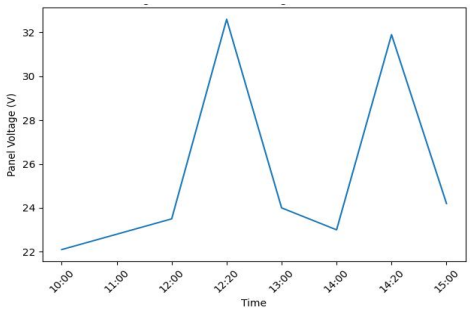

Fig. 15. Panel Voltage versus Time

Fig. 15 shows voltage degradation during soiling periods and a sharp recovery immediately after each cleaning cycle, confirming the effectiveness of the automated cleaning mechanism.

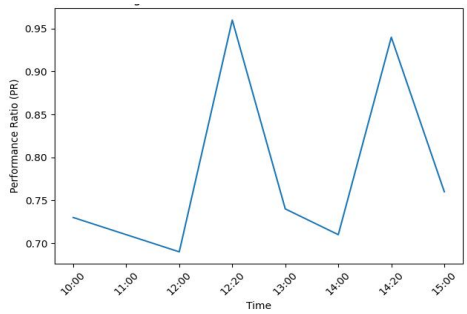

Fig. 16. PR versus Time

Fig. 16 shows that the PR drops below the threshold (0.75) during soiling events and rises sharply after cleaning, validating the reliability of PR-based soiling detection and decision-making.

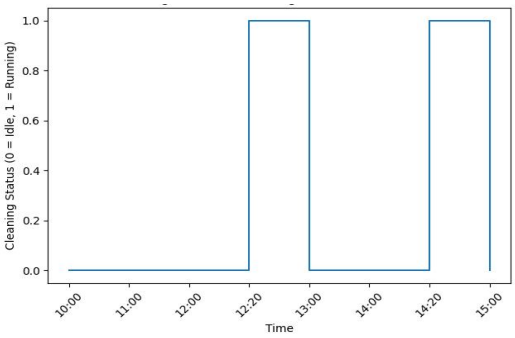

Fig. 17. Cleaning Status Timeline

Fig. 17 illustrates that the timeline visually correlates cleaning operations with PR drops, demonstrating autonomous system response without human intervention.

V. CONCLUSIONS

The proposed IoT-based PV cleaning system effectively mitigates performance losses due to panel soiling through a Performance Ratio (PR)-based comparative detection approach that accurately identifies dust accumulation and activates cleaning only when required. Experimental evaluation demonstrated a restoration of approximately 20–40% of lost output power, confirming the technical effectiveness of the intelligent cleaning mechanism under varying environmental conditions. The system operates autonomously with integrated safety controls to prevent overcurrent, mechanical obstruction, and unnecessary actuation, thereby ensuring reliable and secure operation. In addition, real-time cloud-based monitoring provides continuous tracking of electrical parameters and PR values, enabling remote diagnostics and data-driven maintenance. Overall, the integration of IoT-enabled monitoring with adaptive automated cleaning significantly enhances energy yield, operational reliability, and long-term cost efficiency for residential and commercial photovoltaic installations.

REFERENCES

[1] M. Suleiman, D. K. Joshi, B. Muhammad, and I. Bello, “Performance improvement of PV modules under the effect of partial shading using bil-bot wiping mechanism,” Int. J. Recent Eng. Res. Dev., vol. 9, no. 4, pp. 108–116, 2024.
[2] A. O. Maka and J. M. Alabid, “Solar energy technology and its roles in sustainable development,” Clean Energy, vol. 6, no. 3, pp. 476–483, 2022.
[3] S. Shaik et al., “Experimental analysis on the impacts of soil deposition and bird droppings on the thermal performance of photovoltaic panels,” Case Stud. Therm. Eng., vol. 48, 103128, 2023.
[4] M. J. Alshareef, “A comprehensive review of the soiling effects on PV module performance,” IEEE Access, vol. 11, pp. 134623–134651, 2023.
[5] T. Pivem et al., “Application of a computer vision method for soiling recognition in photovoltaic modules for autonomous cleaning robots,” Signal Image Process. Int. J., vol. 10, no. 3, pp. 43–59, 2019.
[6] J. Sment and A. Zolan, “Status quo and gap analysis of heliostat field deployment processes,” J. Solar Energy Eng., vol. 146, no. 6, 061004, 2024.
[7] H. Abdulla, A. Sleptchenko, and A. Nayfeh, “Optimizing cleaning schedules for spatially distributed photovoltaic installations,” Renew. Energy, vol. 248, 122971, 2025.
[8] M. S. Yahya et al., “Implementation of a real-time IoT based energy management system,” J. Eng. Res. Rep., vol. 25, no. 10, pp. 19–29, 2023.
[9] H. A. Kazem et al., “A review of dust accumulation and cleaning methods for solar photovoltaic systems,” J. Cleaner Prod., vol. 276, 123187, 2020.
[10] S. Gochhait et al., “Application of IoT: A study on automated solar panel cleaning system,” in Proc. 4th Int. Conf. Electrical, Control and Instrumentation Eng. (ICECIE), 2022, pp. 1–4.
[11] M. Anderson et al., “Robotic device for cleaning photovoltaic panel arrays,” in Mobile Robotics: Solutions and Challenges, pp. 367–377, 2010.
[12] M. T. Grando et al., “Robots for cleaning photovoltaic panels: State of the art and future prospects,” Rev. Tecnología y Ciencia, no. 35, pp. 137–150, 2019.
[13] L. Zhou, Y. Jiang, X. Zhang, and Y. Zhai, “An AI-based solar panel cleaning system,” J. Renewable Energy, vol. 177, pp. 275–281, 2021.
[14] I. J. Khan, M. Akhlaq, and F. Qasim, “Removal of dust particles from solar panels using fuzzy logic,” Pak. J. Emerg. Sci. Technol., vol. 3, no. 1, pp. 1–12, 2022.
[15] V. Tiwari, S. Kumari, and P. P. Sahoo, “Monitoring and control of PV microgrid using IoT,” in Proc. 7th Int. Conf. Electrical Energy Systems (ICEES), 2021, pp. 292–298.

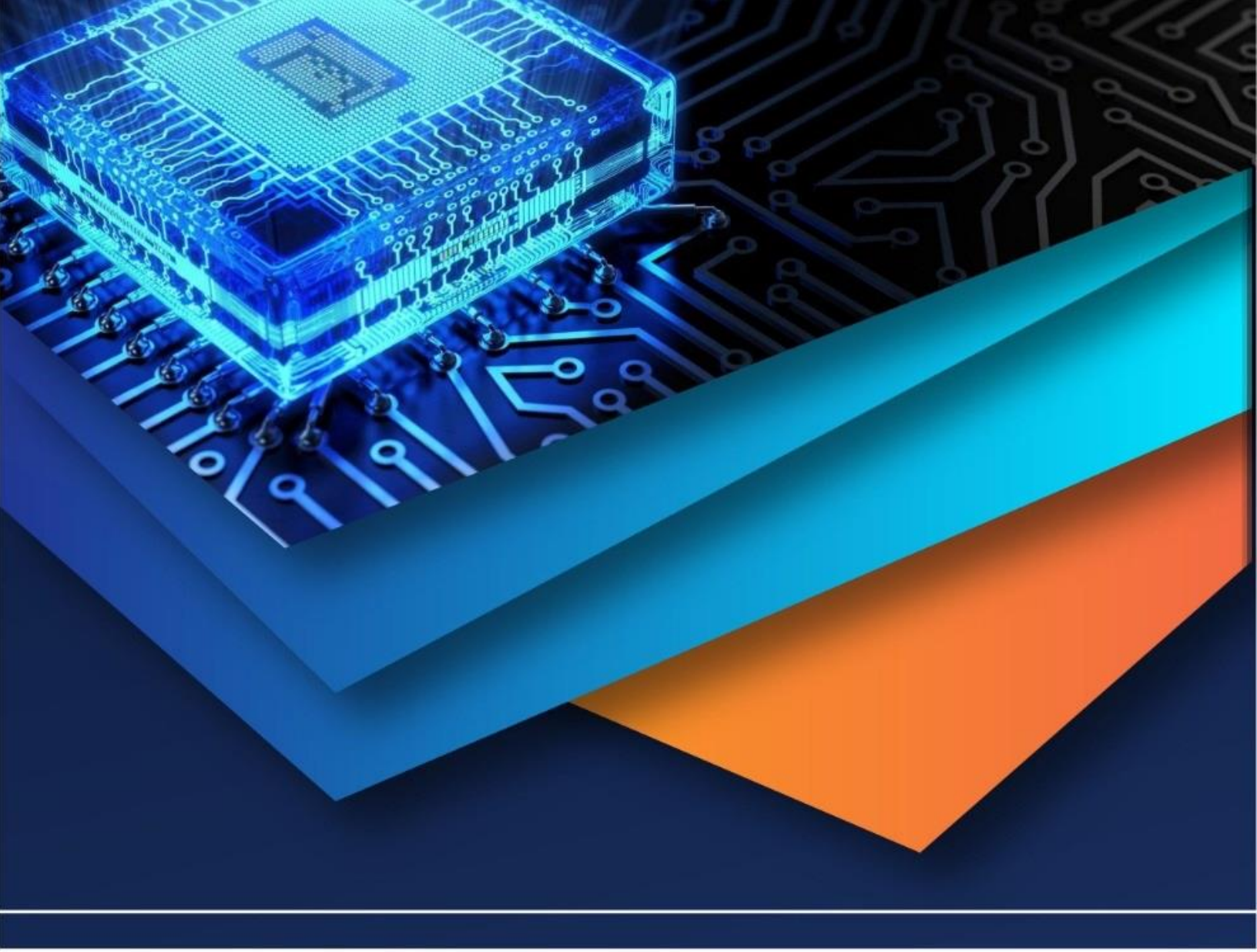

10.22214/IJRASET

45.98

IMPACT FACTOR: 7.129

IMPACT FACTOR: 7.429

INTERNATIONAL JOURNAL FOR RESEARCH

IN APPLIED SCIENCE & ENGINEERING TECHNOLOGY